

The Arc in the DX Cha Circumbinary System: Evidence For a Retrograde Circumbinary Disk

CHENG CHEN ^{1,2}, DANIELA PAZ IGLESIAS ¹, JAMES M. MILEY ^{3,4,5,6,7} AND C.J. NIXON ¹

¹*School of Physics and Astronomy, University of Leeds, Sir William Henry Bragg Building, Woodhouse Ln., Leeds LS2 9JT, UK*

²*Department of Physics and Astronomy, Bishop's University 2600 Rue College, Sherbrooke, QC J1M 1Z7, Canada*

³*Departamento de Física, Universidad de Santiago de Chile, Avenida Victor Jara 3659, Santiago, Chile*

⁴*Millennium Nucleus on Young Exoplanets and their Moons (YEMS), Chile*

⁵*Center for Interdisciplinary Research in Astrophysics and Space Exploration (CIRAS), Universidad de Santiago, Chile*

⁶*Joint ALMA Observatory, Alonso de Córdova 3107, Vitacura, Santiago, Chile*

⁷*European Southern Observatory, Alonso de Córdova 3107, Vitacura, Santiago, Chile*

ABSTRACT

Observations of the binary system DX Cha (HD 104237) reveal a compact, asymmetric ring structure with a radius of 0.43 au. This ring is just outside the binary orbit, which has semi-major axis $a_b = 0.22$ au and eccentricity $e_b = 0.665$; placing the ring at ≈ 1.2 times the binary apocenter distance. The inner regions of circumbinary disks, $\approx 2 - 3 a_b$, are typically evacuated by strong gravitational torques from the binary, resulting in a deep gap between the binary and the disk. Accordingly, previous numerical simulations of DX Cha have found an eccentric inner cavity with almost no material inside ≈ 1 au, and we find similar results when making the same assumption that the circumbinary disk orbits in the same direction as the binary. However, the disk can exist much closer to the binary if it is retrograde. For DX Cha we find that the inner edge of a retrograde disk occurs at $\approx 2a_b$, and moreover takes the form of one or two arcs, in agreement with observations. We therefore suggest that the circumbinary disk in the DX Cha system could be orbiting retrograde to the binary star system in the center. We conclude that compact circumbinary disks observed in young stellar systems are important targets for future observations; if the disks are prograde then their properties are likely to be significantly different from current estimates, while if they are retrograde then this will have profound implications for our understanding of star and planet formation.

Keywords: Stellar accretion disks (1579) – Retrograde orbit (2327) — Accretion (14) — Computational astronomy (293) — Close binary stars (254) — Exoplanet formation (492)

1. INTRODUCTION

The interaction between a binary system and an external accretion flow is a complex process (e.g. Lin & Papaloizou 1986; Pringle 1991; Artymowicz & Lubow 1994). The disk flow tries to move inwards towards the binary through the action of a viscosity (Pringle & Rees 1972; Lynden-Bell & Pringle 1974; Shakura & Sunyaev 1973), which is typically mediated by magnetic fields resulting in hydromagnetic turbulence (Shakura & Sunyaev 1973; Balbus & Hawley 1991). The binary, however, attempts to arrest the disk inflow by transferring energy and angular momentum to the disk orbits through orbital resonances (cf. Lynden-Bell & Kalnajs 1972; Papaloizou & Pringle 1977; Goldreich & Tremaine

1979). The structure of the inner disk regions depends strongly on the competition between these effects and also on the disk properties which affect, for example, where the transferred energy and angular momentum is deposited in the disk (Lubow & Pringle 1993; Korycansky & Pringle 1995; Lubow & Ogilvie 1998; Bate et al. 2002, see Heath & Nixon 2020 for a recent discussion). For typical disk-binary parameters the inner disk regions are depleted of material, and accretion on to the binary takes place via time-dependent streams, which fuel internal disks around each star (e.g. Artymowicz & Lubow 1996).

However, this picture of binary-disk interaction assumes that the binary and disk orbit in the same direction. If instead, the binary rotates in the opposite direction to the disk then the orbital resonances are either drastically reduced in strength for eccentric binaries

(Nixon & Lubow 2015; Ivanov et al. 2015) or absent altogether for circular binaries (Nixon et al. 2011a). In this case, the disk can viscously inflow towards the binary until the inner disk edge is strongly perturbed from a circular orbit by the passing star, typically the lower-mass secondary star. For circular binaries, the material from the disk inner edge is either captured directly by the secondary star into a circumsecondary disk or gravitationally perturbed towards the primary star ending up in a circumprimary disk (Nixon et al. 2011a), while for eccentric binaries it can be dragged in and expelled outwards on the timescale of the binary orbit (Nixon & Lubow 2015). The formation of a retrograde circumbinary disk can occur through a combination of precession and dissipation of a misaligned disk that is initially closer to retrograde than prograde, i.e. the angle between the disk and binary angular momentum vectors is $90^\circ < \theta < 180^\circ$ (Nixon et al. 2011b).⁸ The difference in dynamics between prograde and retrograde disks leads to a significant difference in the structure of the disk near the inner disk edge around the binary.

Misaligned disks are likely to form in different astrophysical environments. For example, in the centers of merged galaxies disks may form with essentially random inclinations around a supermassive black hole binary (Nixon et al. 2011a,b, 2013; Roedig & Sesana 2014; Dunhill et al. 2014). However, in nearby star forming regions the initial conditions for star formation are also highly chaotic and turbulent (Bate et al. 2003; McKee & Ostriker 2007), which is conducive to the formation of misaligned circumbinary disks around young stars (Nixon et al. 2013; Bate 2018). Indeed, observations indicate that such misalignments are common (e.g., Chiang & Murray-Clay 2004; Winn et al. 2004; Kennedy et al. 2012; Brinch et al. 2016), and in some cases polar disks have been found (Kennedy et al. 2019; Kraus et al. 2020). Population studies have found that there is a transition in the present-day alignment properties of circumbinary disks with the orbital period of the binary; for periods less than ~ 100 days almost all circumbinary disks are coplanar with the binary, whereas for longer period systems a substantial fraction of disks are strongly misaligned to the binary orbit (Czekala et al. 2019).

⁸ The criterion is more complex in the case that the disk angular momentum, J_d , is not small compared to the binary angular momentum, J_b , in which case the requirement for the disk to settle into a retrograde orbit is $\cos\theta < -J_d/2J_b$ (Nixon et al. 2011b). Additionally, for sufficiently eccentric binaries with disks that are sufficiently close to 90° inclinations, the stable configuration for the disk may be polar in which the disk angular momentum vector aligns to the binary eccentricity vector (Aly et al. 2015).

Circumbinary disks can be found around many types of young binary systems, including systems containing Herbig Ae stars. These are a subclass of pre-main sequence stars characterized by their intermediate mass, typically ranging from $1.5 - 3 M_\odot$. They are commonly found in star-forming regions and exhibit emission line features from circumstellar environments, often possessing circumstellar disks composed of gas and dust, resulting in an infrared excess in their spectral energy distributions (Brittain et al. 2023; Nidhi et al. 2023). DX Chamaeleontis (DX Cha, HD 104237) is a pre-main-sequence spectroscopic binary with a short period $T_b \simeq 19.859$ days corresponding to a semi-major axis of $a_b = 0.22$ au (Böhm et al. 2004). This system has been observed and comparatively well-studied for more than 20 years by spectroscopic and infrared interferometric observations (e.g. Leinert et al. 2003; Böhm et al. 2004; Grady et al. 2004; Tatulli et al. 2007; Garcia et al. 2013; Cowley et al. 2013; Bailer-Jones et al. 2021; Juhász et al. 2025). The binary consists of a Herbig Ae star with a mass of $2.2 M_\odot$ and a K3 star with a mass of $1.4 M_\odot$ (Grady et al. 2004; Garcia et al. 2013). The two stars are in an eccentric orbit with $e_b = 0.665$ (Böhm et al. 2004). Prior work constrains the binary orbital orientation on the sky and indicates that the disk is viewed close to face-on (Garcia et al. 2013). However, the relative prograde or retrograde sense between the binary and the disk remains uncertain in the absence of resolved disk kinematics. The system is surrounded by a circumbinary disk of mass $M_d = 0.04 M_\odot$ estimated by modeling the disk spectral energy distribution (SED; Hales et al. 2014). Due to its near face-on geometry, this system provides an ideal case for detailed studies of the accretion process in young binary systems. Here we are specifically interested in the emission on small scales around the binary system.

Garcia et al. (2013) report a tidal truncation radius of the circumbinary disk around DX Cha at ≈ 0.44 au ($2a_b$) from analyzing data from the Very Large Telescope Interferometer (VLTI)/AMBER in the K -band continuum and the $\text{Br}\gamma$ line. To understand the disk-binary interaction in DX Cha, Dunhill et al. (2015) performed numerical simulations of a prograde circumbinary disk, finding that the asymmetric cavity around the binary is large, with diameter of ≈ 4 au which is significantly larger than suggested by the observations presented by Garcia et al. (2013). Although the simulations in Dunhill et al. (2015) suggest there could be an accretion stream attached to both stars within the cavity, Juhász et al. (2025) fit more recent L -band ($3.55 \mu\text{m}$) data from the Multi Aperture Mid-Infrared Spectroscopic Experiment (MATISSE) on VLTI and find a best-fit of an azimuthally asymmetric

narrow ring structure (width ~ 0.13 au) with a diameter of 0.86 au. [Juhász et al. \(2025\)](#) conclude that the data shows material orbiting within a circumbinary disk rather than spiraling on to the stars from within a cavity. However, this is at odds with the circumbinary disk structure found in simulations ([Dunhill et al. 2015](#)), and might be more in line with the structures formed from a retrograde circumbinary disk.

To test this possibility, we present Smoothed Particle Hydrodynamics (SPH) simulations of prograde and retrograde circumbinary disks with parameters appropriate to the DX Cha system to see which can provide a better fit to the structures inferred from the observations. In Section 2 we describe the model setup of our simulations. We present our simulation results in Section 3. Finally, we present our discussion in Section 4, and conclusions in Section 5.

2. NUMERICAL SETUP

To investigate the DX Cha system, we employ the SPH code PHANTOM ([Price et al. 2018](#)) which has been widely used for studying circumbinary systems (starting with [Nixon 2012](#)). We adopt the binary system parameters from Table 1 in [Juhász et al. \(2025\)](#): the total binary mass M_b is composed of the primary mass $M_1 = 2.2M_\odot$, and the secondary mass $M_2 = 1.4M_\odot$. The binary eccentricity is $e_b = 0.665$, and the separation of the binary is $a_b = 0.22$ au.

We set up an accompanying circumbinary disk coplanar with the binary and with the disk material initially following circular orbits. The total disk mass is initially $M_d = 10^{-3}M_b$. The disk initially extends from $R_{\text{in}} = 3a_b$ to $R_{\text{out}} = 10a_b$, and is comprised of $N_{\text{p,ini}} = 5 \times 10^6$ particles. This choice of M_d serves as a fiducial normalization and is of the same order as the mean disk mass inferred from CO emission modeling ([Stapper et al. 2024](#)). However, our simulated disk is truncated at $R_{\text{out}} \approx 2.2$ au, which is much smaller than the CO-traced disk extent of ≈ 40 au reported for DX Cha ([Stapper et al. 2024](#)); therefore, the adopted M_d in our setup should not be interpreted as the total disk mass on ~ 40 au scales. We use a small outer disk radius to focus the resolution of our simulation on the inner regions where the disk–binary interaction predominantly occurs. In general, the choice of M_d does not affect the disk evolution unless it is sufficiently high that the disk self-gravity becomes important (which occurs when $M_d/M_b \gtrsim H/R$; [Pringle 1981](#)). We do not include the gas self-gravity in our simulations and thus, while the binary orbit is held fixed, we can rescale the disk mass if required. However, when allowing the binary orbit to evolve, the value of the disk mass does

affect the binary orbital evolution. We return to this point in Sec. 4.2.

We set the outer boundary condition as zero-torque, which means that any particles with $R > R_{\text{out}}$ are removed along with their angular momentum. The accretion radii of both stars R_{acc} are initially set to $0.4a_b$ to reduce the computational cost of reaching the disk’s quasi-steady state at larger radii. Once this state is reached, we reduce R_{acc} for each star to 0.1 of its effective Roche lobe radius. This is given by ([Eggleton 1983](#))

$$R_L = \frac{0.49q_b^{2/3}}{0.69q_b^{2/3} + \ln(1 + q_b^{1/3})} a_b. \quad (1)$$

Thus, R_{acc} for the primary and the secondary are $0.0389a_b$ and $0.0320a_b$, respectively. With these smaller accretion radii, the gas flows around each star can be resolved.⁹

We use a locally isothermal equation of state for the gas through a modified form of the prescription suggested by [Farris et al. \(2014\)](#) for circumbinary disks. The sound speed c_s depends on the distance from the primary star, r_1 , and the secondary star, r_2 , and is given by

$$c_s = hR_{\text{in}}^q \frac{(M_1/r_1 + M_2/r_2)^q}{(M_1 + M_2)^q} \sqrt{\frac{GM_b}{R_{\text{in}}}}, \quad (2)$$

where we use a disk sound speed power-law index of $q = 0.25$ and h is the disk angular semi-thickness at R_{in} which we take to be 0.05.

The initial surface density $\Sigma(R)$ is set from the steady-state solution to the 1D disk diffusion equation with mass added to the disk at a rate \dot{M}_{add} to keep it steady at a radius $R_{\text{add}} = 7a_b$. This is done via the method outlined in the Appendix of [Drewes & Nixon \(2021\)](#), but here we set the initial velocity of the injected particles to be the velocity of their nearest neighboring particles, rather than the local Keplerian velocity.

The physical viscosity is modeled by a Navier-Stokes viscosity corresponding to a Shakura-Sunyaev disk viscosity parameter $\alpha_{\text{SS}} = 0.1$ ([Shakura & Sunyaev 1973](#)). For the numerical viscosity, we use a variable linear viscosity coefficient with $\alpha_{\text{min}} = 0.01$ and $\alpha_{\text{max}} = 1$. The

⁹ Typically the accretion radii used in numerical simulations are significantly larger than the physical size of the objects being simulated. However, in this case, using a stellar mass-radius relation of $R_*/R_\odot = (M_*/M_\odot)^{0.8}$, the accretion radii of 0.1 times the Roche lobe is very close to the actual stellar radius. The magnetic field of the stars could redirect the flow at several stellar radii (e.g. [Bouvier et al. 2007](#)). We do not account for this effect in our simulations, but we note that the structures we are interested in are on scales outside of the binary orbit and thus unlikely to be significantly affected by the stellar magnetic field.

value of the linear coefficient is set via a modified Cullen & Dehnen (2010) switch (see Price et al. 2018, for details). For the quadratic numerical viscosity, we take $\beta_{\text{SPH}} = 2\alpha_{\text{SPH}}$ (e.g. Chen & Nixon 2025).

Our simulations allow material to accrete on to each of the stars. However, to create a quasi-steady-state disk structure¹⁰, we initially do not include the back reaction from the disk on to the binary evolution. Once a steady state is reached we allow the back reaction to determine the subsequent evolution of the binary orbit. The timescale on which the disk reaches this state is the viscous timescale $t_\nu = R^2/\nu$, where $\nu = \alpha_{\text{SS}}(H/R)^2 R^2\Omega$. Based on these parameters, the disk is expected to reach a steady state after a time $\sim 10,000T_b$, where T_b is the binary orbital period.

3. SIMULATION RESULTS

First we note that the prograde and retrograde disk simulations reach a quasi-steady-state after $\approx 5,000$ and $\approx 5,500$ binary orbits respectively. This is slightly quicker than expected in part due to the presence of numerical viscosity which slightly augments the physical viscosity included in the simulations. At this stage we are still employing a relatively large accretion radius as described above to reduce computational cost. We therefore change the sink particle accretion radii, to 0.1 of their respective Roche lobe radii, and continue the simulation until a new quasi-steady-state is reached.

We describe the resulting disk structures in the subsections below, with the prograde case first and then followed by the retrograde case.

3.1. Prograde case

Once the prograde disk reached the final state, the number of particles in the disk has increased to ≈ 6155000 . In the left panel of Fig. 1, we plot the column density of the steady-state prograde disk when the two stars are at nearly apoapsis (from now on, we redefine time as $t = t' - t_{\text{std}}$, where t' denotes the code time and t_{std} is the time when the system reaches a steady state). The axes are given in units of the binary semi-major axis, and the units for the column density color bar are arbitrary. The tidal interaction between the binary and the circumbinary disk results in an eccentric inner cavity with an apocenter of around $\approx 4a_b$ (0.88 au) and the shortest radius $\approx 2a_b$ (0.44 au) to the mass center of the binary. This size agrees with Hirsh et al.

(2020) who found a similar cavity size with similar parameters (see their Fig. 9). The most significant density enhancement occurs at a radius of around $\approx 4.5 a_b$ (towards the bottom left in the left panel of Fig. 1) which coincides with the apocenter of the eccentric inner edge of the circumbinary disk. There is also a spiral from the inner edge of the circumbinary disk feeding mass into the circumprimary disk.

The location of the density enhancement at the apocenter of the eccentric inner edge of the circumbinary disk precesses around the binary with time (MacFadyen & Milosavljević 2008). In Fig. 2, we plot a series of snapshots with time intervals of about $100 T_b$. The position angle of the enhancement region evolves over time and it takes about $500 T_b$ to complete a full revolution around the binary. Throughout this precession, the inner cavity maintains its asymmetric structure and remains at a large distance from the binary.

To understand the cavity evolution on shorter timescales, we plot in Fig. 3 a series of snapshots of the disk structure with an interval of $0.1T_b$. We also mark on the plot with two cyan dashed circles, the location and width (utilizing the full width at half maximum, FWHM) of the ring modeled in Juhász et al. 2025. During the disk evolution, one or two spirals transit through this region, but with significantly lower density than the disk inner edge at much larger radii.

3.2. Retrograde case

Once the retrograde disk reached the final state, the number of particles in the disk has increased to ≈ 5920000 , which is slightly fewer than the prograde case. In the right panel of Fig. 1, we plot the column density of the retrograde disk once it has reached a quasi-steady-state (here we also define time $t = 0$ from this snapshot). Compared to the prograde circumbinary disk in the left panel, the retrograde disk has a smaller inner cavity with a radius $\approx 2a_b$ and the cavity is also more symmetric, dominated by an $m = 2$ mode (as opposed to the prograde case which is dominated by an $m = 1$ mode; see Nixon & Lubow 2015 for details).

The smaller cavity is as expected for the retrograde case in which the tidal torque from the binary is significantly weaker (see the figures in Nixon et al. 2011a; Nixon 2012; Nixon & Lubow 2015). Our results are similar to the lower-left panel of Figure 6 in Nixon & Lubow (2015) as this is the closest match to the parameters employed here. Looking at Figures 4-6 in Nixon & Lubow (2015), we can see that for small $q \leq 0.3$ there is a single prominent arc, while for larger q the structure is comprised of two arcs.

¹⁰ Here *quasi* refers to the fact that the binary orbit still induces time dependence to the disk structure. However, by averaging over (a small multiple of) the binary orbital period, the disk properties have reached a steady state.

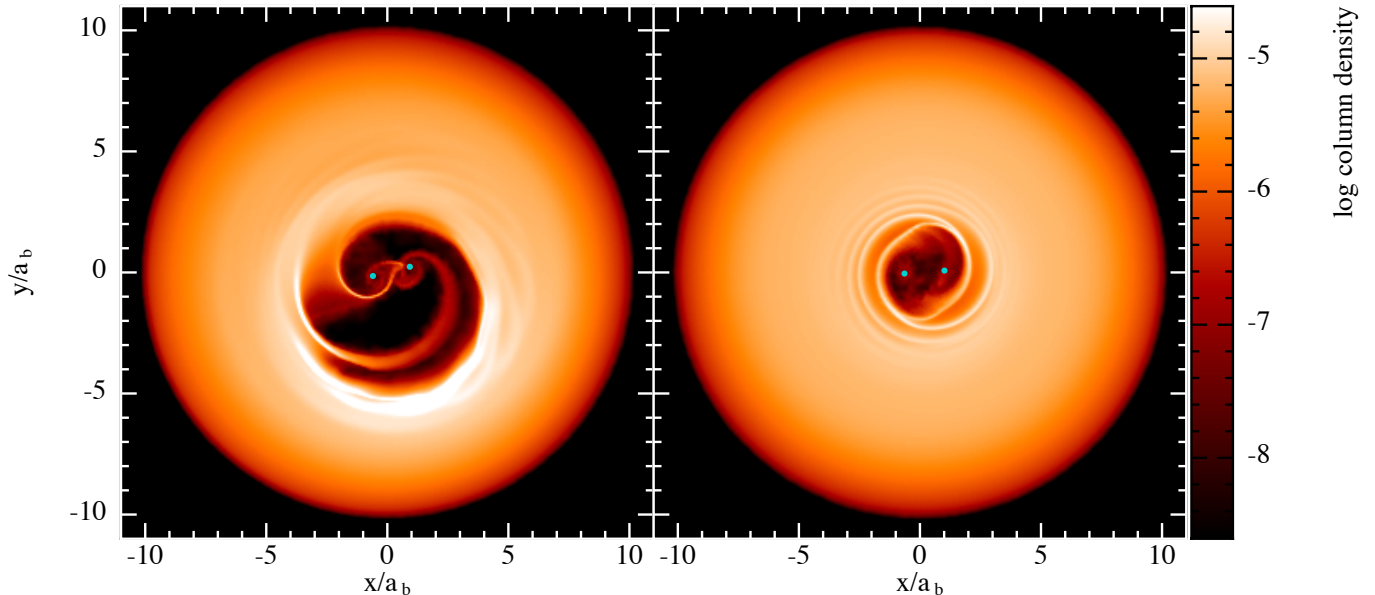


Figure 1. Column density profiles for prograde (left) and retrograde (right) circumbinary disks once they have each reached a quasi-steady state. In each panel, the left cyan point represents the primary and the right cyan point represents the secondary. In the prograde case we see a large inner cavity has been evacuated which is punctuated by a stream that feeds the circumprimary disk. The strongest density enhancement in this case occurs at a radius of around $4 - 5a_b$. In the retrograde case the disk extends much closer to the binary with a ring-like structure occurring at around $2a_b$ with a thickness of around $0.5a_b$. The retrograde disk structure is in better agreement with the observations for DX Cha.

In Fig. 4, which is the same as Fig. 2 but for the retrograde case, we show that the disk structure in the retrograde case does not change substantially over long timescales. In this case the arcs are formed from material that is accelerated by interaction with the stars, predominantly at apocenter; this means that the phase angle of the arcs does not change significantly with time.

As in Fig. 3 for the prograde case, we also plot in Fig. 5 the retrograde case throughout a binary orbit with intervals between snapshots of $0.1T_b$. Again the two cyan dashed circles represent the location and FWHM of the ring modeled by Juhász et al. (2025). Two approximately symmetric spirals with a phase difference of $\approx 180^\circ$ are launched outward from the material interacting directly with the binary. The innermost material encroaches right on to the binary, while the density peak in the arcs occurs at around $2a_b$ (0.44 au). This simulation is consistent with the analytic model of Nixon & Lubow (2015), which predicts that the strongest dimensionless mode $S_{-1,2}$ occurs at $\approx 2a_b$. The spiral arcs observed in the retrograde circumbinary disk simulation occupy the general area indicated by the data as modeled by Juhász et al. (2025).

4. DISCUSSION

4.1. Prograde or retrograde?

The size and structure of the cavity around the binary is strongly affected by whether the circumbinary

disk is prograde or retrograde. Previous simulations of prograde circumbinary disks conclude that the cavity size is $\sim 3 - 5a_b$ for values of q_b and e_b that are similar to those of DX Cha (e.g. Thun & Kley 2018; Hirsh et al. 2020; Penzlin et al. 2024). This translates to a size of ~ 1 au, which is significantly larger than implied by the observations (e.g. Juhász et al. 2025).

Indeed, Dunhill et al. (2015) explicitly modeled DX Cha and found a cavity size that is too large for this system. We have also simulated a prograde circumbinary disk with larger $\alpha_{SS} = 0.1$ to see if a larger disk viscosity can prevent the formation of a large inner cavity. However, the cavity in our simulation is still strongly asymmetric and significantly wider than observed. Moreover, two asymmetric spirals cannot explain the azimuthally asymmetric narrow ring structure modeled from observations. The density enhancement region located at $4.5 a_b$ ($\simeq 1$ au) is still too far from the ring's location. Additionally, the period of the position angle of the enhancement region is more than $400 T_b$. This precession rate of the disk $\dot{\omega}$ at $R = 4.5 a_b$ is similar to the calculation in Leung & Lee (2013) for a test particle orbiting around a binary that

$$\dot{\omega} \simeq \frac{3}{4} \frac{M_1 M_2}{(M_1 + M_2)^2} \left(\frac{a_b}{R} \right)^2 \left(1 + \frac{e_b}{2} \right)^2. \quad (3)$$

With the parameters from our simulation, we found $\dot{\omega} \simeq 0.75^\circ$ per T_b and thus it takes about $480 T_b$ for

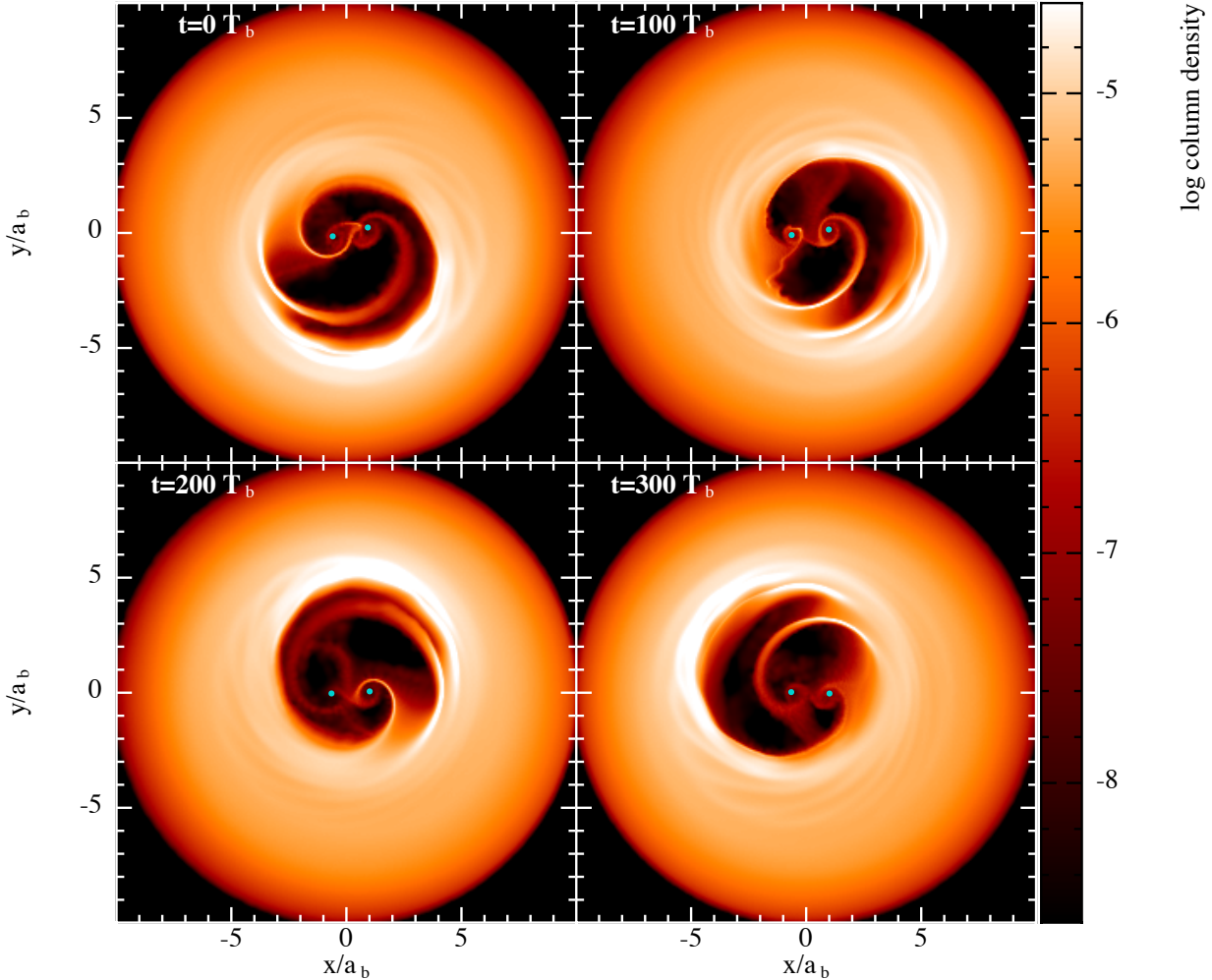


Figure 2. Series of snapshots showing the precession of the density enhancement at the apocentre of the eccentric inner disk edge. The snapshots are spaced by around $100T_b$, and the timescale for a full precession of the enhancement is $\approx 500T_b$ for these parameters. The inner disk structure is not fixed, but varies through the binary orbit; this is shown in more detail in Fig. 3.

the enhancement region to complete one orbit. On the other hand, in Figure 3 of Juhász et al. (2025), they found that the ring varies its position angle very fast between their observational epoch 1 and 2 (see equations 4 and 5 of Juhász et al. 2025). Consequently, neither the spirals nor the density enhancement region can fit the ring structure for the prograde disk.

Alternatively, the disk in DX Cha might be prograde but possess parameters significantly distinct from those we have employed here. Specifically, Heath & Nixon (2020) demonstrated that prograde disks with large $H/R = 0.2$ and high viscosity $\alpha_{ss} = 0.3$ can avoid resonance-driven truncation, allowing the disk to extend much closer to the binary. However, in this scenario, we should observe two prominent symmetric spirals and an azimuthally symmetric rings at the inner edge of circumbinary disk. Moreover, achieving such a

large H/R requires extreme physical conditions. Since $H/R \approx c_s/v_k$, a high H/R implies a very high sound speed relative to the Keplerian velocity, v_k . For the DX Cha system ($M_b = 3.6 M_\odot$), at a distance of $R \approx 1$ au, v_k is ~ 56 km/s. To sustain $H/R \approx 0.2$, c_s must be 11 km/s. Even if we consider that the inner disk region is hot and fully ionized, resulting in a low mean molecular weight of $\mu \approx 0.6$ (as noted by Martin et al. 2019) and we assume m_p to be the proton mass and the Boltzmann constant is k_b , the required temperature would be $T \approx \mu m_p c_s^2 / k_b \approx 9000$ K. This temperature is significantly higher than typical protoplanetary disk temperatures at 1 au, which are generally limited by dust sublimation (~ 1500 K) or stellar irradiation equilibrium.

Regarding viscosity, we used $\alpha_{ss} = 0.1$, which is already at the upper end of estimates for fully ionized disks (Martin et al. 2019) and motivated partly by nu-

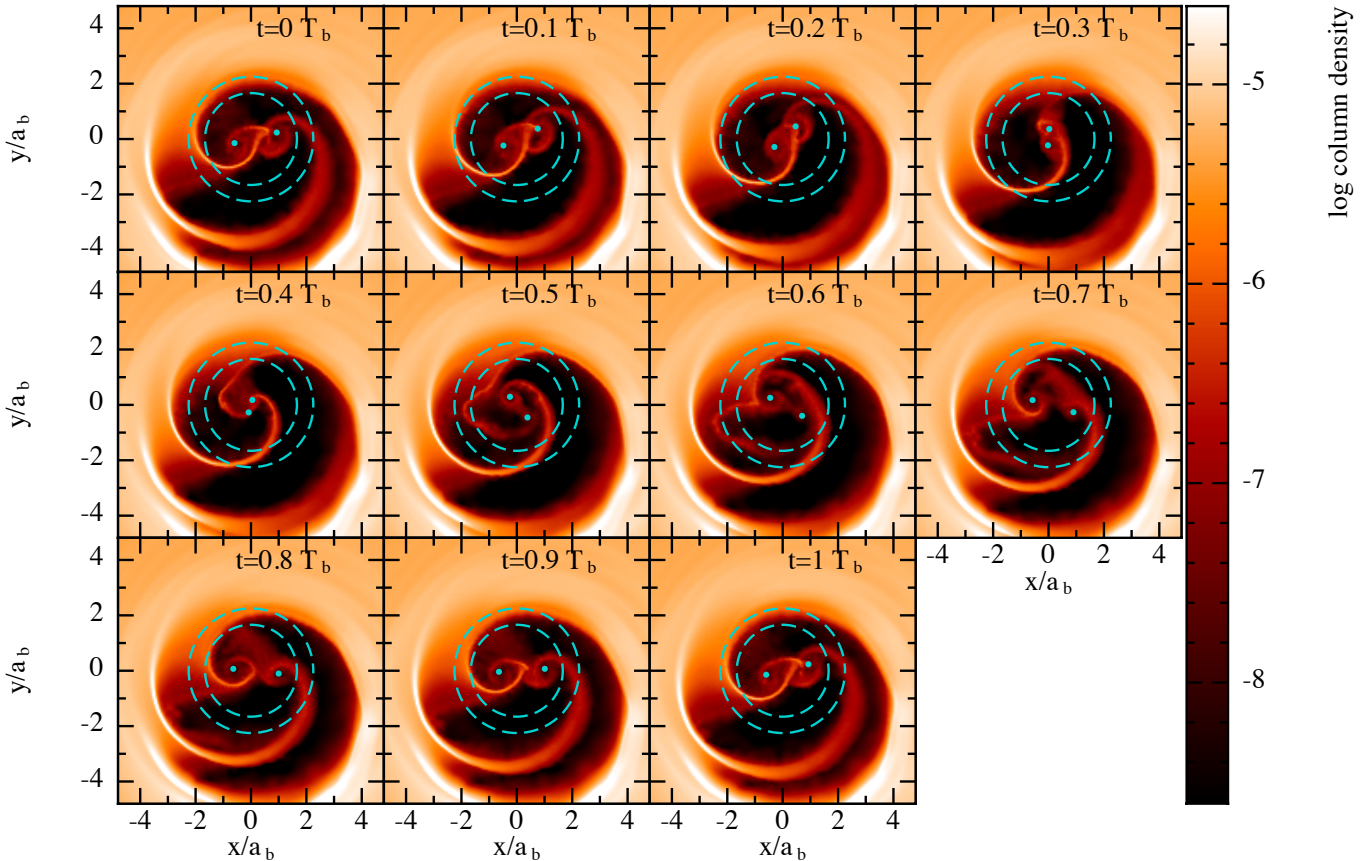


Figure 3. Series of snapshots showing the disk structural changes on short timescales as the binary completes an orbit. Each panel is separated in time by an interval of $0.1T_b$. The two cyan dashed circles indicate the location and FWHM of the azimuthal asymmetric ring modeled in Juhász et al. (2025). While the spiral streams can cross the location of the observed ring, the strong density enhancement associated with the inner edge of the circumbinary disk is at a significantly larger radius than the observed ring.

merical convenience. Protoplanetary disks are typically expected to have lower viscosity (e.g. Hartmann et al. 1998; Rosotti 2023), which would result in even larger cavities (Dunhill et al. 2015). Therefore, while a prograde disk with extreme scale height and viscosity could theoretically fit the spatial scale of the cavity, the physical conditions required ($T \sim 10^4$ K at 1 au) are unlikely to be sustained in the DX Cha system.

Furthermore, the proximity of the disk inner edge to the binary (~ 1 au) implies high gas temperatures. Based on our simulation parameters, the temperature in this region is $T \sim 3000$ K. At such temperatures, dust sublimation occurs and thermal ionization of alkali metals becomes important, likely activating the Magnetorotational Instability (MRI; e.g. Jankovic et al. 2021, 2022). While we do not explicitly simulate magnetohydrodynamics (MHD), our choice of a high viscosity α_{ss} effectively captures the angular momentum transport driven by MRI turbulence in this ionized regime (Martin et al. 2019). Previous comparisons between MHD and hydrodynamical simulations of circumbinary

disks indicate that the cavity size is largely governed by the balance between binary torques and viscous spreading, yielding similar results when the effective stress is matched (e.g. Shi et al. 2012). Since higher viscosity leads to a smaller cavity (Dunhill et al. 2015), and our high α_{ss} prograde model still produces a cavity significantly larger than observed, explicitly including magnetic field effects is unlikely to reconcile the prograde scenario with observations. Thus, the hydrodynamic approximation with high α_{ss} serves as a robust upper limit for the ability of a prograde disk to encroach upon the binary.

Finally, we address the impact of thermodynamics. Our simulations employ a locally isothermal equation of state (modified from Farris et al. 2014), which is a common approximation but neglects radiative cooling and detailed energy transport. Recent studies have explored circumbinary disk evolution with more sophisticated thermodynamics (e.g. Sudarshan et al. 2022; Pierens & Nelson 2023; Penzlin et al. 2024). These works generally find that while radiative effects can alter

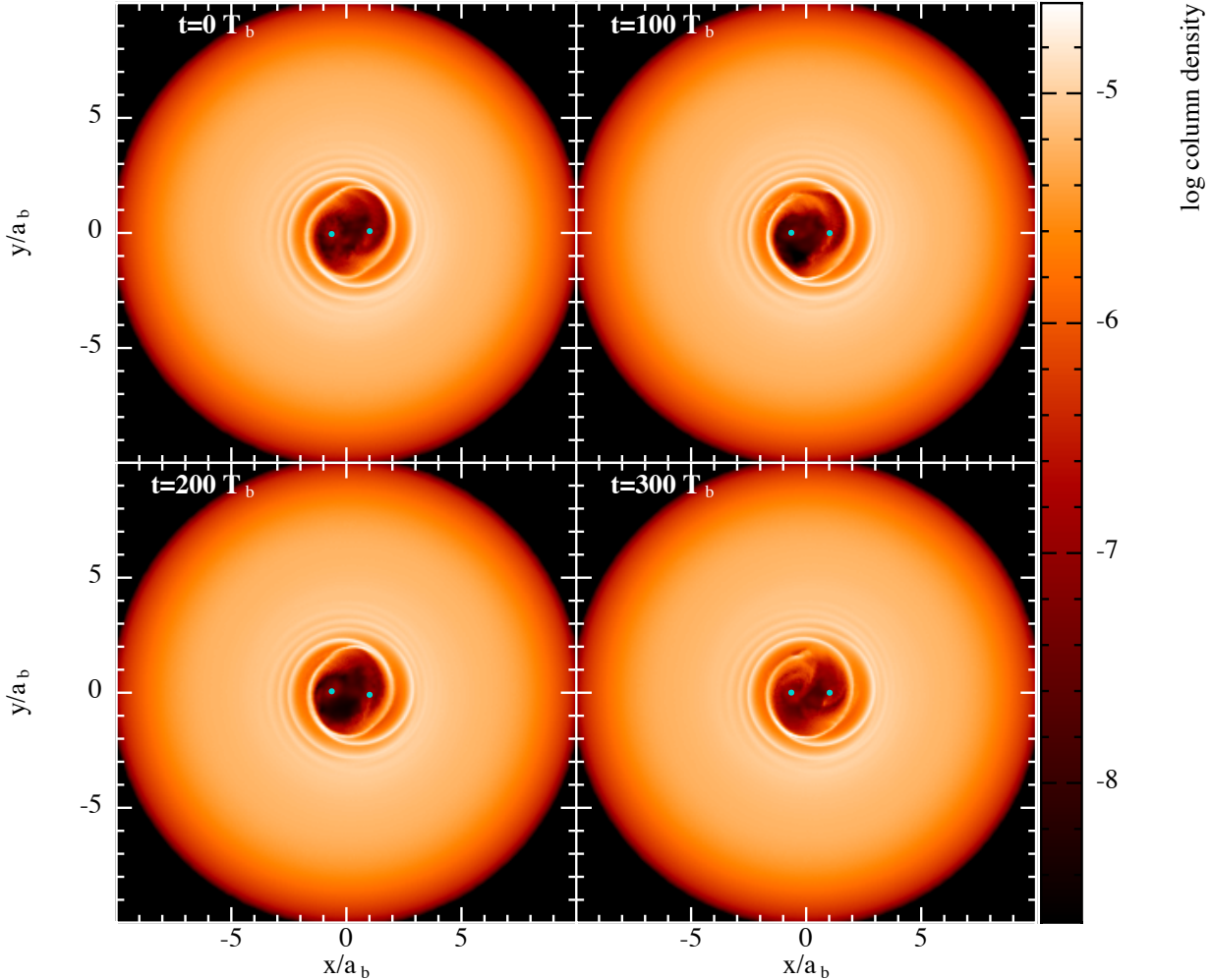


Figure 4. Same as Fig. 2 except for the retrograde, rather than prograde, case.

the cavity eccentricity and density contrast, they do not drastically reduce the cavity size for prograde binaries with significant eccentricity.

In fact, if radiative cooling leads to a cooler disk (lower H/R), the cavity size in the prograde case often increases or remains large because orbital resonances become stronger in thinner disks (Pierens & Nelson 2023). Conversely, confirming the findings of Sudarshan et al. (2022), no thermodynamic treatment has yet demonstrated the ability to shrink the inner cavity of a prograde disk around an eccentric binary ($e_b \sim 0.665$) to the size inferred for DX Cha ($\approx 2 a_b$). Therefore, while including more complex thermal physics might refine the detailed shape of the arcs in our retrograde models, it is unlikely to enable the prograde scenario to match the compact ring structure observed.

Based on our retrograde circumbinary disk simulation, we infer that DX Cha hosts a retrograde circumbinary disk instead of a prograde circumbinary disk for several

reasons. First, eccentric resonances in a retrograde circumbinary disk produce a relatively small and symmetric inner cavity, which has similar features to those reported in previous observations. Second, two symmetric spirals propagate from outward, and their surface densities evolve to the brightest values around $2 a_b$ (0.44 au). This result matches the radius of the asymmetric ring modeled in Juhász et al. (2025). Further, Juhász et al. (2025) employed a model with only a first order azimuthal modulation (see Lazareff et al. 2017, for details). This means that the model is restricted to only one maximum brightness and one brightness minimum in the opposite direction over the azimuthal range. As the size of this ring is significantly smaller than previous prograde simulations had suggested, Juhász et al. (2025) concluded that the ring corresponds to material orbiting within the cavity rather than the inner edge of the circumbinary disk. However, Figure 14 in Lazareff et al. (2017) shows that χ^2 for the second order modula-

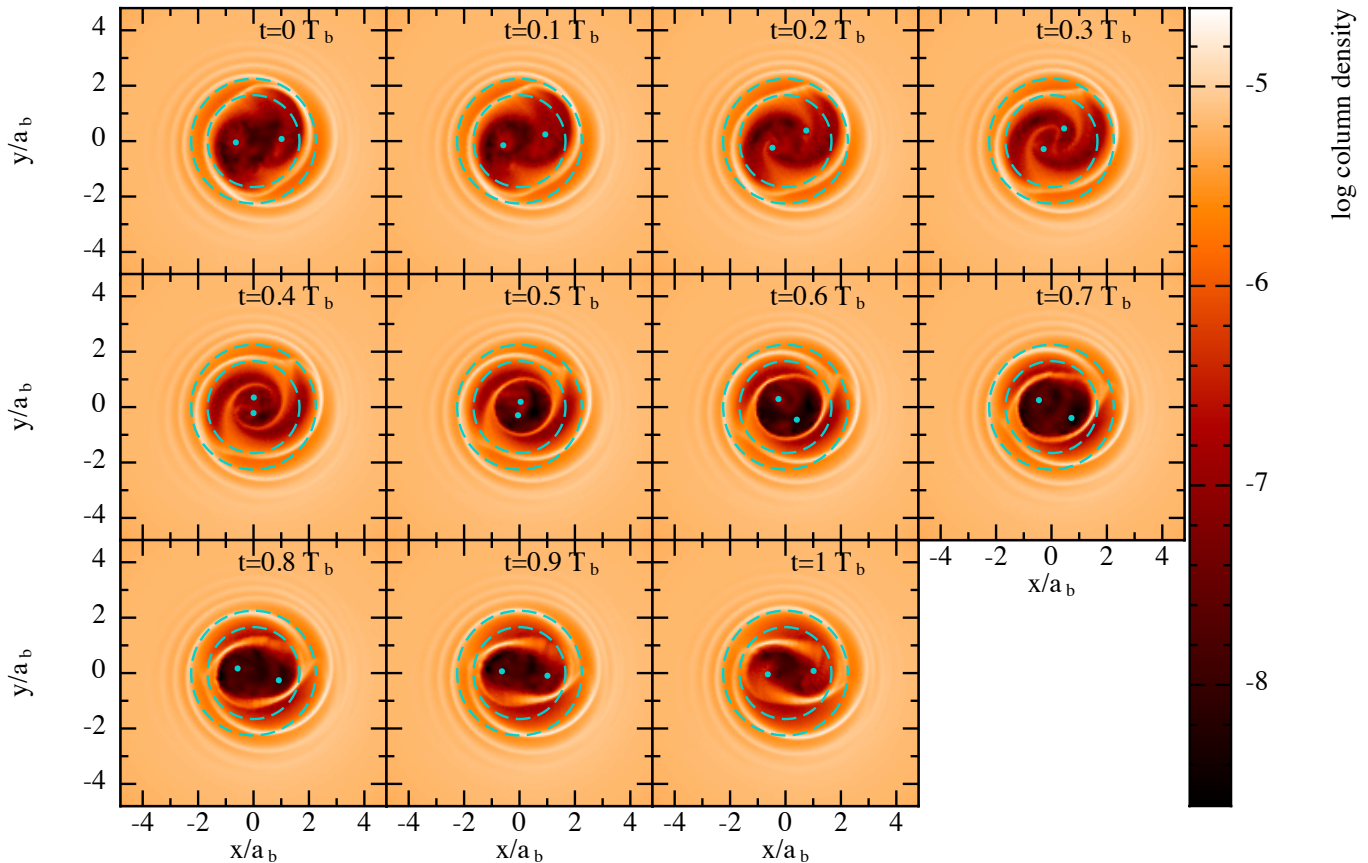


Figure 5. Same as Fig. 3 except for the retrograde, rather than prograde, case.

tion in some disk systems can be smaller than those with the first order modulation. Thus, we suggest that the asymmetric double spiral present in the retrograde case may be a good fit to the data for the azimuthal structure of the ring. On the other hand, given the sparse uv-coverage of the VLTI/MATISSE observations, the image presented in Juhász et al. (2025) should be interpreted as the image of a best-fitting parametric brightness model constrained by the interferometric observables measured at the available uv points, rather than a unique image reconstruction. Consequently, higher-complexity structures (e.g. multi-armed spirals) are not uniquely required by the available data and would be difficult to justify without substantially improved uv-coverage. In this work, we therefore restrict our comparison to robust, low-order morphological properties (ring radius/width and low-order azimuthal asymmetry) that are directly captured by the adopted parametric models.

Additionally, it is worth mentioning that the time interval between the second and third observations in Juhász et al. (2025) ($16.02 T_b$) is nearly a full orbital period of the binary. Hence, the rings fitted in Figure 3 of Juhász et al. (2025) for these two observations are very similar. On the other hand, the difference in ring

positions between the first and second observations in the same figure is due to the time interval between these two observations not being close to a full T_b . As a result, they fitted two different rings in these two observations. Moreover, the phase angle difference between two rings in the first and second observations is about 180° which is consistent with our simulation result.

Finally, according to the fitting parameters in Juhász et al. (2025), the amplitudes of the azimuthal modulation in three observation epochs are $(A_{mod1}, A_{mod2}, A_{mod3}) = (0.77, 0.47, 0.98)$, respectively. These three values indicate the degree of asymmetry of rings they modeled and the ratio of the brightness minimum to the maximum brightness of rings can be calculated by $(1 - A_{mod}) / (1 + A_{mod})$. Hence, the ratios for the three observations are 0.13, 0.36, and 0.01, respectively. Because the column density can be used to infer the brightness, in Fig. 6, we convert Fig. 1 into polar coordinates, and the two cyan vertical lines represent the FWHM of the ring reported in Juhász et al. (2025). For the prograde case on the left panel, the ratio of the brightness minimum to the maximum brightness within the region of two lines is $\ll 10^{-2}$ due to the deeper cavity while the ratio of the retrograde case is $\gtrsim 10^{-2}$ principally due

to the shallow cavity. Consequently, the retrograde simulation provides a better explanation of the degree of asymmetry measured by Juhász et al. (2025) than the prograde one.

As the orbital direction of the DX Cha binary has been confirmed (Garcia et al. 2013), the most straightforward way to determine whether DX Cha hosts a retrograde circumbinary disk is through observational data that reveals the kinematic substructures of the disk (e.g. Teague et al. 2021). For moderately inclined disks with optically thick CO observed at high angular resolution, the emitting surfaces of both the front and back side of the disk can be spatially separated in individual ALMA channels (e.g. Pinte et al. 2018a,b; Law et al. 2022; Izquierdo et al. 2023). In such cases we can thereby distinguish the near- and far-side of the disk using the ALMA data. However, this cannot yet be achieved for DX Cha with current ALMA observations. In fact it is particularly difficult given the almost face-on inclination with respect to the observer ($i \sim 20^\circ$; Czekała et al. 2019), in combination with a relatively compact protoplanetary disk ($R_{\text{out}} \approx 40$ au; Stapper et al. 2024) meaning that ALMA’s longest baselines (nominal configuration 10) would be required to angularly resolve this separation. Scattered light observations are equally challenged by the face-on inclination of the source, in which the amount of reflected light received by the observation will be minimized.

4.2. Accretion rate of DX Cha

In our simulations, we turn off the back reaction of the binary from the circumbinary disk in order to prevent the orbital evolution of the binary before the circumbinary disk reaches a steady state. To study the orbital evolution of DX Cha and the binary precession due to the disk, we need to turn on the switch to allow the binary to feel the circumbinary disk. However, the disk mass will play a role in affecting these circumbinary disk-induced evolutions.

Therefore, to set the value of the disk mass in our simulations, M_d , more precisely, we fit the average accretion rate measured from 93 spectroscopic observations of DX Cha’s main component collected from the ESO (European Southern Observatory) archive. We followed the methodology described in Iglesias et al. (2023), where the mass accretion rate is estimated from the intensity of the H α line emission at 6562.85Å. The net H α emission intensity can be quantified in terms of its equivalent width as $\text{EW}_{\text{emi}} = \text{EW}_{\text{obs}} - \text{EW}_{\text{abs}}$, where EW_{obs} is the EW of the observed H α spectrum, and EW_{abs} is the EW of the intrinsic H α absorption. We fit a Kurucz model to the wings of the H α line to esti-

mate the EW_{abs} . The best-fit model was achieved for $T_{\text{eff}} = 7250$ K, $\log(g) = 4.6$ dex, and $v \sin i = 20$ km s $^{-1}$, adopting solar metallicity and turbulent velocity of 2.0 km s $^{-1}$. The net H α emission flux is then estimated as $F_{\text{emi}} = \text{EW}_{\text{emi}} \times F_\lambda$, where F_λ is the expected flux at the center of the H α line. We estimated F_λ by using the Kurucz model and scaling it by $(D/R_\star)^2$, where $D = 106.6$ pc is the distance to the star (Gaia Collaboration et al. 2021) and $R_\star = 2.67R_\odot$ is the main component’s stellar radius, estimated following Iglesias et al. (2023). Then, the emission line luminosity L_{emi} is calculated as $L_{\text{emi}} = 4\pi D^2 F_{\text{emi}}$, and the accretion luminosity L_{acc} is calculated in terms of L_{emi} by following the relationship from Mendigutía et al. (2011):

$$\log\left(\frac{L_{\text{acc}}}{L_\odot}\right) = A + B \times \log\left(\frac{L_{\text{emi}}}{L_\odot}\right) \quad (4)$$

where $A = 2.09 \pm 0.06$ and $B = 1.00 \pm 0.05$ are the relationship values for H α obtained by Fairlamb et al. (2017). Finally, following Wichittanakom et al. (2020), the mass accretion rate \dot{M}_{acc} is determined from L_{acc} , R_\star , and stellar mass M_\star as:

$$\dot{M}_{\text{acc}} = \frac{L_{\text{acc}} R_\star}{GM_\star} \quad (5)$$

In the left panel of Fig 7, we show \dot{M}_{acc} epochs, which varies widely, ranging from $\sim 10^{-8}$ $M_\odot \text{yr}^{-1}$ to $\sim 4 \times 10^{-7}$ $M_\odot \text{yr}^{-1}$. We take the average value of 2.26×10^{-7} $M_\odot \text{yr}^{-1}$. This accretion rate is consistent with typical values observed for Herbig Ae/Be stars (Wichittanakom et al. 2020).

For our retrograde simulations, \dot{M}_{acc} at a steady state is about $\sim 4.76 \times 10^{-5}$ $M_\odot \text{yr}^{-1}$. Hence, we divide both M_d and \dot{M}_{add} by a factor of 200 and restart the simulation for more than 1000 days. In the right panel of Fig 7, we show that the accretion rate with the time of the primary (blue dashed line) and the secondary (yellow dashed line) of DX Cha with the time after we changed M_d in first 500 days. The green line represents the sum of the blue line and the yellow line, and the mean total \dot{M}_{acc} is $\sim 2.29 \times 10^{-7}$ $M_\odot \text{yr}^{-1}$, which is comparable to the mean value in the left panel.

4.3. Orbital evolution of DX Cha

In Fig. 8, we plot a_b versus time for prograde (blue), retrograde (yellow dashed) and retrograde with lower M_d (green dot-dashed) cases. All of these three cases show that the binary’s orbit shrinks over time. However, the \dot{a}_b of retrograde case is faster than the prograde case by an order of magnitude. Because particles in the retrograde circumbinary disk provide the negative specific angular momentum as they accrete onto a binary

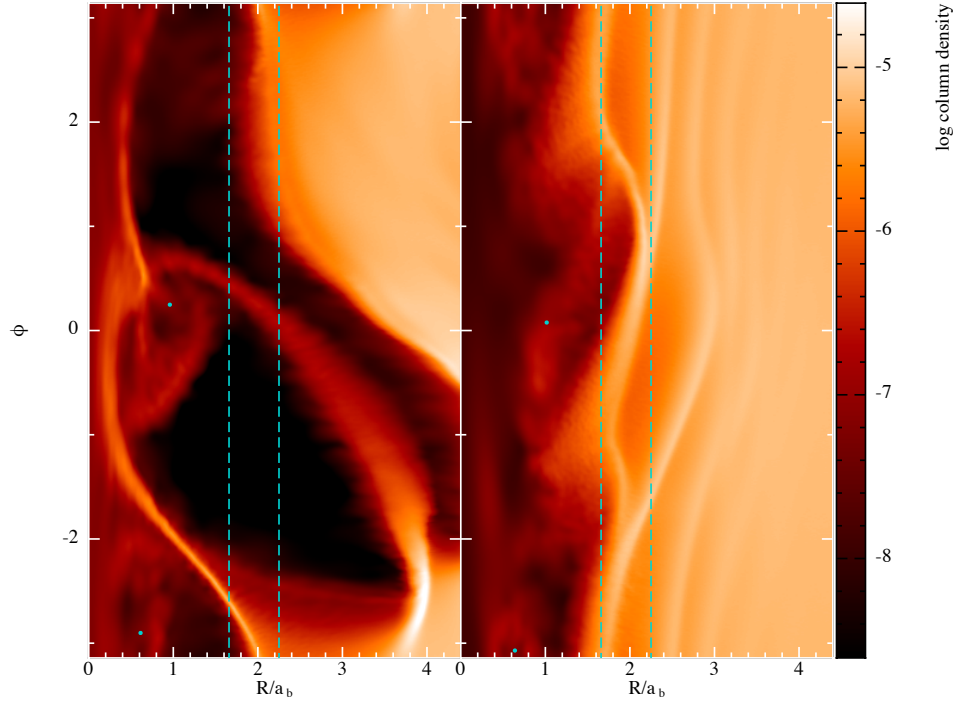


Figure 6. Same as Fig. 1 except viewed in polar coordinates, R, ϕ , and showing a smaller range in R . The prograde case is on the left and the retrograde case is on the right. The two cyan vertical lines indicate the FWHM of the azimuthal asymmetric ring modeled in Juhász et al. (2025).

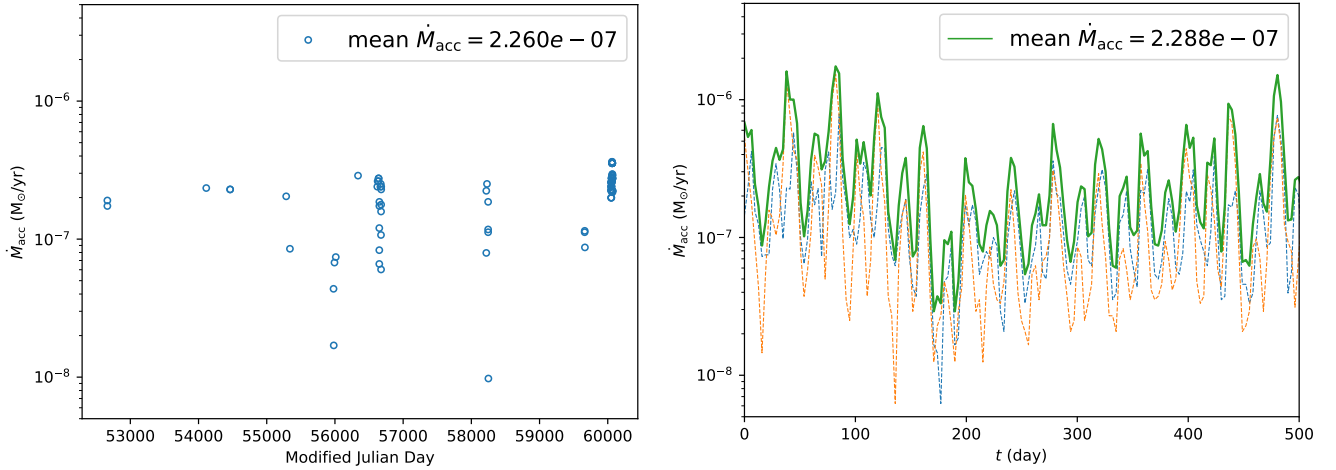


Figure 7. *Left:* The fitting results of \dot{M}_{acc} of DX Cha across the 93 epochs shown as empty circles. *Right:* The new \dot{M}_{acc} of DX Cha with the time in our simulations after we reduce the disk mass in our model from the original value given in the setup (Section 2) by a factor of ≈ 200 . The blue and orange dashed lines represent \dot{M}_{acc} of the primary and the secondary of DX Cha in the retrograde simulation, respectively. The green line is the total \dot{M}_{acc} .

star, it can speed up the shrinkage rate of the binary (Nixon et al. 2011a, 2013; Nixon & Lubow 2015).

Furthermore, by comparing slopes of yellow dashed and green dot-dashed lines, we confirm that a_b can be scaled down by M_d in our simulations. Hence, if we convert the time unit into years, our results suggest that DX Cha may merge within 2 million years.

However, in addition to the binary-disk interaction, the tidal interaction between the two stars must be considered because the binary separation is only 0.22 au. The n -body simulation in Chen et al. (2024) shows that an eccentric binary with $e_b = 0.8$ and $a_b = 0.2$ au will merge eventually within $120,000 T_b$. Importantly, in their simulation, they employed the constant time lag approximation, which does not evolve the spins of either star (Baronett et al. 2022, § 3.1). On the other hand, the observation of the young ($\sim 10^6$ yr) Orion OB1c/d association rotation periods of (Stassun et al. 1999) show that the majority of rotation periods of those stars are ≤ 8 days which is much smaller than the orbital period of DX Cha (~ 20 days). As a result, the tidal interaction of DX Cha would cause the binary to expand over time if two stars are not tidally locked. Thus, to investigate this topic, we will (in the future) perform n -body simulations with the spin evolution for both stars. Combining the binary-disk interaction and the tidal interaction of the binary, we will be able to determine the net effect of the orbital evolution of DX Cha and estimate the shrinkage or expansion rate correctly.

Furthermore, since the phase angle of the spiral in the retrograde circumbinary disk depends on the argument of periapsis of the binary (ω_b), it can vary with time due to interactions with the circumbinary disk. Therefore, we plot the time evolution of ω_b in the right panel of Fig. 8 which shows that the variation of ω_b is $< 0.006^\circ$ within $400 T_b$. This implies that the evolution of the spiral’s phase angle generated from the retrograde circumbinary disk does not vary significantly within several hundred T_b . Consequently, model fitting results from future VLTI observations may reveal their position angles depending on the observational epochs.

4.4. Retrograde circumbinary planet formation

Currently, only 16 circumbinary planets have been detected by Kepler and TESS databases (Doyle et al. 2011; Welsh et al. 2012; Orosz et al. 2012a,b; Kostov et al. 2014; Welsh et al. 2015; Li et al. 2016; Kostov et al. 2016, 2020; Socia et al. 2020) and they are all close to coplanar and prograde with the binary orbital plane. However, recent observations reported that a polar planet around the 2MASS J15104786-2818174 binary system (Baycroft et al. 2025). This finding implies that planet forma-

tion can also occur in misaligned circumbinary disks. While polar circumbinary gas disks such as HD 98800 (Kennedy et al. 2019), V773 Tau B (Kenworthy et al. 2022) and a polar circumbinary debris disk around the binary 99 Herculis (Kennedy et al. 2012; Smallwood et al. 2020) have been found, a retrograde circumbinary disk has not yet been discovered. Retrograde circumbinary disks may be rarer than their prograde counterparts in the universe for a variety of reasons, including their formation mechanism, which may require more extreme environments (e.g., substantial late infall of misaligned material or capturing a star with opposing orbital momentum, see Kuffmeier et al. 2021; Pelkonen et al. 2025; Hühn et al. 2025 for details), and because the lifetime of retrograde disks may be shorter than similar prograde disks as the material is not held out by resonances in the retrograde case (e.g., Nixon et al. 2011a; Nixon & Lubow 2015).

Planet formation in a retrograde circumbinary disk should be similar to that in a prograde circumbinary disk. In both prograde and retrograde circumbinary disks, a planet located beyond $5a_b$ can be quite stable (Doolin & Blundell 2011; Chen et al. 2020). However, due to planet migration (either type I or type II) a circumbinary planet (CBP) could migrate to the inner edge of the circumbinary disk. As a result, a prograde circumbinary planet may be unstable if its semi-major axis $< 3 a_b$, although some theories suggest that a CBP within the inner unstable region will move outward to the innermost stable region due to a balance of orbital excitation from the central stars and the gas-drag force (Yamanaka & Sasaki 2019).

Compared to planet formation in prograde circumbinary disks, retrograde circumbinary disks can provide a relatively stable environment for planetesimal growth near the inner edge. Furthermore, n -body simulations show that massive retrograde CBPs can be more stable than prograde CBPs in low and moderate e_b systems (e.g. Chen et al. 2020). Hence, if we detect a CBP between 1.5 to 2.5 a_b in a binary system with a low or middle e_b , on stability grounds we can expect that it is on a retrograde orbit. On the other hand, although our simulations suggest that a tenuous mini-disk could form around one of stars, its lifetime is quite short. Furthermore, there is no observational evidence of mini-disks in the DX Cha system potentially due to the effects of both stellar wind and stellar magnetic field (Garcia et al. 2013). Hence, we infer that our simulations are not able to answer whether the DX cha system host a mini disk and more complicated models are required to deal with this problem.

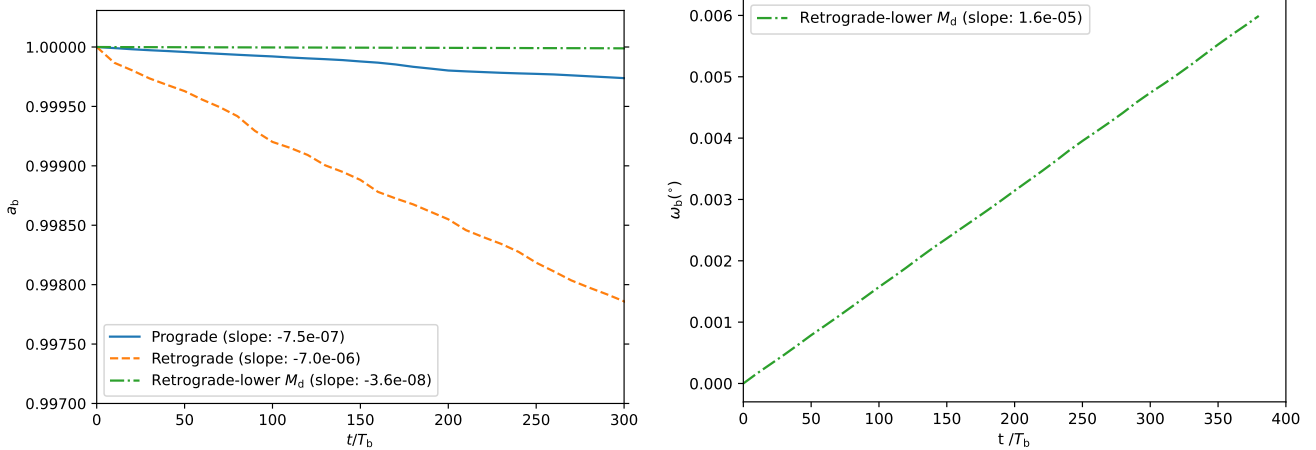


Figure 8. *Left:* a_b versus T_b for prograde (blue), retrograde (orange dashed) and retrograde with the lower M_d (green dot-dashed) cases. The slopes in the legend indicate the \dot{a}_b rates for three simulations. *Right:* Time evolution of ω_b for the retrograde disk simulation.

5. CONCLUSION

In this study, we perform SPH simulations to investigate whether the observed structures of the DX Cha circumbinary disk are more consistent with prograde or retrograde rotation of the disk. When the disk is prograde, we find an asymmetric inner cavity extending out to several times the binary semi-major axis, with only low density streams making it to the binary orbit. The strongest density enhancement occurs in a region located at $\approx 4.5a_b$, and which has a precession time of about $500T_b$. This is too large a radial scale to be able to explain the asymmetric ring structure observed for DX Cha by VLTI/MATISSE observations (see left panel of Fig. 1).

On the other hand, for the retrograde case, the disk extends much closer to the binary orbit and forms a more symmetric inner cavity that might appear as an asymmetric ring in current analysis of the available observational data. The disk inner edge is located almost exactly where the observations indicate; two spiral arcs are launched and the density peaks at around $2a_b$ (0.44 au; see right panel of Fig. 1). Moreover, in both cases the precession of the high-density features takes place on significantly longer timescales than inferred from changes in the phase of the asymmetric ring reported Juhász et al. (2025); while this cannot be explained with a prograde disk or through precession of the binary orbit in the retrograde case, it might be explained by the sub-orbital timescale evolution of the arcs formed around the binary in the retrograde case (see Fig. 5).

We therefore suggest that DX Cha hosts a retrograde circumbinary disk. This claim can be verified, or falsified, by future observations that confirm the direction of the disk’s rotation vector. This can be done, for ex-

ample, using spatially and velocity resolved kinematics from molecular lines (e.g. Calcino et al. 2024). However, achieving sufficient spatial resolution for this system may be challenging.

We therefore draw the conclusion that detailed observations of compact circumbinary disks around young stellar binaries are an excellent way of advancing our understanding of the physics of disk-binary interaction, which plays a fundamental role in many astrophysical systems from star and planet formation to evolution in stellar mass compact object binaries to supermassive black hole mergers.

Additionally, the environment of DX Cha may play a role in determining the formation of any planets in the circumbinary disk. Grady et al. (2004) show that there are several nearby stars indicating that DX Cha may have undergone a flyby that could truncate or disrupt the circumbinary disk affecting the disk’s ability to form planets or the orbits of any planets that have already formed.

Finally, to investigate the orbital interaction between the binary and the disk, we rescaled the mass of the disk by fitting the $H\alpha$ flux of DX Cha across 93 observational epochs. With the rescaled disk mass, the binary-disk interaction leads to the binary’s orbit shrinking over time, and the binary may merge within 2 million years (cf. Chen et al. 2024). However, DX Cha consists of pre-main sequence stars, which usually have faster spin rates than their orbital period. Hence, to determine the real orbital evolution of the binary, the tidal interactions of the two stars have to be taken into account.

ACKNOWLEDGEMENTS

We thank Isaac Radley, John Ilee, Catherine Walsh and Melvin Hoare for useful discussions. CC, CJN and DI acknowledge support from the Science and Technology Facilities Council (grant numbers ST/Y000544/1 and ST/X001016/1). CC acknowledges support from the CITA National Fellowship (grant number DIS-2022-568580). CJN acknowledges support from the Leverhulme Trust (grant number RPG-2021-380). This project has received funding from the European Union's

Horizon 2020 research and innovation program under the Marie Skłodowska-Curie grant agreement No 823823 (Dustbusters RISE project). We acknowledge the use of resources provided by the Isambard 3 Tier-2 HPC Facility. Isambard 3 is hosted by the University of Bristol and operated by the GW4 Alliance (<https://gw4.ac.uk>) and is funded by UK Research and Innovation; and the Engineering and Physical Sciences Research Council [EP/X039137/1].

REFERENCES

- Aly, H., Dehnen, W., Nixon, C., & King, A. 2015, *MNRAS*, 449, 65, doi: [10.1093/mnras/stv128](https://doi.org/10.1093/mnras/stv128)
- Artymowicz, P., & Lubow, S. H. 1994, *ApJ*, 421, 651, doi: [10.1086/173679](https://doi.org/10.1086/173679)
- . 1996, *ApJL*, 467, L77, doi: [10.1086/310200](https://doi.org/10.1086/310200)
- Bailer-Jones, C. A. L., Rybizki, J., Fouesneau, M., Demleitner, M., & Andrae, R. 2021, *AJ*, 161, 147, doi: [10.3847/1538-3881/abd806](https://doi.org/10.3847/1538-3881/abd806)
- Balbus, S. A., & Hawley, J. F. 1991, *ApJ*, 376, 214, doi: [10.1086/170270](https://doi.org/10.1086/170270)
- Baronett, S. A., Ferich, N., Tamayo, D., & Steffen, J. H. 2022, *MNRAS*, 510, 6001, doi: [10.1093/mnras/stac043](https://doi.org/10.1093/mnras/stac043)
- Bate, M. R. 2018, *MNRAS*, 475, 5618, doi: [10.1093/mnras/sty169](https://doi.org/10.1093/mnras/sty169)
- Bate, M. R., Bonnell, I. A., & Bromm, V. 2003, *MNRAS*, 339, 577, doi: [10.1046/j.1365-8711.2003.06210.x](https://doi.org/10.1046/j.1365-8711.2003.06210.x)
- Bate, M. R., Ogilvie, G. I., Lubow, S. H., & Pringle, J. E. 2002, *MNRAS*, 332, 575, doi: [10.1046/j.1365-8711.2002.05289.x](https://doi.org/10.1046/j.1365-8711.2002.05289.x)
- Baycroft, T. A., Sairam, L., Triaud, A. H. M. J., & Correia, A. C. M. 2025, arXiv e-prints, arXiv:2504.12209, doi: [10.48550/arXiv.2504.12209](https://doi.org/10.48550/arXiv.2504.12209)
- Böhm, T., Catala, C., Balona, L., & Carter, B. 2004, *A&A*, 427, 907, doi: [10.1051/0004-6361:20041227](https://doi.org/10.1051/0004-6361:20041227)
- Bouvier, J., Alencar, S. H. P., Harries, T. J., Johns-Krull, C. M., & Romanova, M. M. 2007, in *Protostars and Planets V*, ed. B. Reipurth, D. Jewitt, & K. Keil, 479, doi: [10.48550/arXiv.astro-ph/0603498](https://doi.org/10.48550/arXiv.astro-ph/0603498)
- Brinch, C., Jørgensen, J. K., Hogerheijde, M. R., Nelson, R. P., & Gressel, O. 2016, *ApJL*, 830, L16, doi: [10.3847/2041-8205/830/1/L16](https://doi.org/10.3847/2041-8205/830/1/L16)
- Brittain, S. D., Kamp, I., Meeus, G., Oudmaijer, R. D., & Waters, L. B. F. M. 2023, *SSRv*, 219, 7, doi: [10.1007/s11214-023-00949-z](https://doi.org/10.1007/s11214-023-00949-z)
- Calcino, J., Norfolk, B. J., Price, D. J., et al. 2024, *Monthly Notices of the Royal Astronomical Society*, 534, 2904, doi: [10.1093/mnras/stae2233](https://doi.org/10.1093/mnras/stae2233)
- Chen, C., Baronett, S. A., Nixon, C. J., & Martin, R. G. 2024, *Monthly Notices of the Royal Astronomical Society: Letters*, 533, L37, doi: [10.1093/mnrasl/slae058](https://doi.org/10.1093/mnrasl/slae058)
- Chen, C., Lubow, S. H., & Martin, R. G. 2020, *MNRAS*, 494, 4645, doi: [10.1093/mnras/staa1037](https://doi.org/10.1093/mnras/staa1037)
- Chen, C., & Nixon, C. J. 2025, *MNRAS*, 540, 2465, doi: [10.1093/mnras/staf881](https://doi.org/10.1093/mnras/staf881)
- Chiang, E. I., & Murray-Clay, R. A. 2004, *ApJ*, 607, 913, doi: [10.1086/383522](https://doi.org/10.1086/383522)
- Cowley, C. R., Castelli, F., & Hubrig, S. 2013, *MNRAS*, 431, 3485, doi: [10.1093/mnras/stt430](https://doi.org/10.1093/mnras/stt430)
- Cullen, L., & Dehnen, W. 2010, *MNRAS*, 408, 669, doi: [10.1111/j.1365-2966.2010.17158.x](https://doi.org/10.1111/j.1365-2966.2010.17158.x)
- Czekala, I., Chiang, E., Andrews, S. M., et al. 2019, *The Astrophysical Journal*, 883, 22, doi: [10.3847/1538-4357/ab287b](https://doi.org/10.3847/1538-4357/ab287b)
- Doolin, S., & Blundell, K. M. 2011, *MNRAS*, 418, 2656, doi: [10.1111/j.1365-2966.2011.19657.x](https://doi.org/10.1111/j.1365-2966.2011.19657.x)
- Doyle, L. R., Carter, J. A., Fabrycky, D. C., et al. 2011, *Science*, 333, 1602, doi: [10.1126/science.1210923](https://doi.org/10.1126/science.1210923)
- Drewes, N. C., & Nixon, C. J. 2021, *ApJ*, 922, 243, doi: [10.3847/1538-4357/ac2609](https://doi.org/10.3847/1538-4357/ac2609)
- Dunhill, A. C., Alexander, R. D., Nixon, C. J., & King, A. R. 2014, *MNRAS*, 445, 2285, doi: [10.1093/mnras/stu1914](https://doi.org/10.1093/mnras/stu1914)
- Dunhill, A. C., Cuadra, J., & Dougados, C. 2015, *MNRAS*, 448, 3545, doi: [10.1093/mnras/stv284](https://doi.org/10.1093/mnras/stv284)
- Eggleton, P. P. 1983, *ApJ*, 268, 368, doi: [10.1086/160960](https://doi.org/10.1086/160960)
- Fairlamb, J. R., Oudmaijer, R. D., Mendigutia, I., Ilee, J. D., & van den Ancker, M. E. 2017, *MNRAS*, 464, 4721, doi: [10.1093/mnras/stw2643](https://doi.org/10.1093/mnras/stw2643)
- Farris, B. D., Duffell, P., MacFadyen, A. I., & Haiman, Z. 2014, *ApJ*, 783, 134, doi: [10.1088/0004-637X/783/2/134](https://doi.org/10.1088/0004-637X/783/2/134)
- Gaia Collaboration, Brown, A. G. A., Vallenari, A., et al. 2021, *A&A*, 649, A1, doi: [10.1051/0004-6361/202039657](https://doi.org/10.1051/0004-6361/202039657)
- Garcia, P. J. V., Benisty, M., Dougados, C., et al. 2013, *MNRAS*, 430, 1839, doi: [10.1093/mnras/stt005](https://doi.org/10.1093/mnras/stt005)

- Goldreich, P., & Tremaine, S. 1979, *ApJ*, 233, 857, doi: [10.1086/157448](https://doi.org/10.1086/157448)
- Grady, C. A., Woodgate, B., Torres, C. A. O., et al. 2004, *ApJ*, 608, 809, doi: [10.1086/420763](https://doi.org/10.1086/420763)
- Hales, A. S., De Gregorio-Monsalvo, I., Montesinos, B., et al. 2014, *AJ*, 148, 47, doi: [10.1088/0004-6256/148/3/47](https://doi.org/10.1088/0004-6256/148/3/47)
- Hartmann, L., Calvet, N., Gullbring, E., & D'Alessio, P. 1998, *ApJ*, 495, 385, doi: [10.1086/305277](https://doi.org/10.1086/305277)
- Heath, R. M., & Nixon, C. J. 2020, *A&A*, 641, A64, doi: [10.1051/0004-6361/202038548](https://doi.org/10.1051/0004-6361/202038548)
- Hirsh, K., Price, D. J., Gonzalez, J.-F., Ubeira-Gabellini, M. G., & Ragusa, E. 2020, *MNRAS*, 498, 2936, doi: [10.1093/mnras/staa2536](https://doi.org/10.1093/mnras/staa2536)
- Hühn, L.-A., Jiang, H.-C., & Dullemond, C. P. 2025, *A&A*, 701, L15, doi: [10.1051/0004-6361/202555391](https://doi.org/10.1051/0004-6361/202555391)
- Iglesias, D. P., Panić, O., van den Ancker, M., et al. 2023, *MNRAS*, 519, 3958, doi: [10.1093/mnras/stac3619](https://doi.org/10.1093/mnras/stac3619)
- Ivanov, P. B., Papaloizou, J. C. B., Paardekooper, S. J., & Polnarev, A. G. 2015, *A&A*, 576, A29, doi: [10.1051/0004-6361/201424359](https://doi.org/10.1051/0004-6361/201424359)
- Izquierdo, A. F., Testi, L., Facchini, S., et al. 2023, *A&A*, 674, A113, doi: [10.1051/0004-6361/202245425](https://doi.org/10.1051/0004-6361/202245425)
- Jankovic, M. R., Mohanty, S., Owen, J. E., & Tan, J. C. 2022, *MNRAS*, 509, 5974, doi: [10.1093/mnras/stab3370](https://doi.org/10.1093/mnras/stab3370)
- Jankovic, M. R., Owen, J. E., Mohanty, S., & Tan, J. C. 2021, *MNRAS*, 504, 280, doi: [10.1093/mnras/stab920](https://doi.org/10.1093/mnras/stab920)
- Juhász, T., Varga, J., Ábrahám, P., et al. 2025, *ApJ*, 982, 36, doi: [10.3847/1538-4357/adb727](https://doi.org/10.3847/1538-4357/adb727)
- Kennedy, G. M., Wyatt, M. C., Sibthorpe, B., et al. 2012, *MNRAS*, 421, 2264, doi: [10.1111/j.1365-2966.2012.20448.x](https://doi.org/10.1111/j.1365-2966.2012.20448.x)
- Kennedy, G. M., Matrà, L., Facchini, S., et al. 2019, *Nature Astronomy*, 3, 278, doi: [10.1038/s41550-019-0715-1](https://doi.org/10.1038/s41550-019-0715-1)
- Kenworthy, M. A., González Picos, D., Elizondo, E., et al. 2022, arXiv e-prints, arXiv:2207.05575, <https://arxiv.org/abs/2207.05575>
- Korycansky, D. G., & Pringle, J. E. 1995, *MNRAS*, 272, 618, doi: [10.1093/mnras/272.3.618](https://doi.org/10.1093/mnras/272.3.618)
- Kostov, V. B., McCullough, P. R., Carter, J. A., et al. 2014, *ApJ*, 784, 14, doi: [10.1088/0004-637X/784/1/14](https://doi.org/10.1088/0004-637X/784/1/14)
- Kostov, V. B., Orosz, J. A., Welsh, W. F., et al. 2016, *ApJ*, 827, 86, doi: [10.3847/0004-637X/827/1/86](https://doi.org/10.3847/0004-637X/827/1/86)
- Kostov, V. B., Orosz, J. A., Feinstein, A. D., et al. 2020, *AJ*, 159, 253, doi: [10.3847/1538-3881/ab8a48](https://doi.org/10.3847/1538-3881/ab8a48)
- Kraus, S., Kreplin, A., Young, A. K., et al. 2020, *Science*, 369, 1233, doi: [10.1126/science.aba4633](https://doi.org/10.1126/science.aba4633)
- Kuffmeier, M., Dullemond, C. P., Reissl, S., & Goicovic, F. G. 2021, *A&A*, 656, A161, doi: [10.1051/0004-6361/202039614](https://doi.org/10.1051/0004-6361/202039614)
- Law, C. J., Crystian, S., Teague, R., et al. 2022, *ApJ*, 932, 114, doi: [10.3847/1538-4357/ac6c02](https://doi.org/10.3847/1538-4357/ac6c02)
- Lazareff, B., Berger, J. P., Kluska, J., et al. 2017, *A&A*, 599, A85, doi: [10.1051/0004-6361/201629305](https://doi.org/10.1051/0004-6361/201629305)
- Leinert, C., Graser, U., Przygodda, F., et al. 2003, *Ap&SS*, 286, 73, doi: [10.1023/A:1026158127732](https://doi.org/10.1023/A:1026158127732)
- Leung, G. C. K., & Lee, M. H. 2013, *ApJ*, 763, 107, doi: [10.1088/0004-637X/763/2/107](https://doi.org/10.1088/0004-637X/763/2/107)
- Li, G., Holman, M. J., & Tao, M. 2016, *ApJ*, 831, 96, doi: [10.3847/0004-637X/831/1/96](https://doi.org/10.3847/0004-637X/831/1/96)
- Lin, D. N. C., & Papaloizou, J. 1986, *ApJ*, 307, 395, doi: [10.1086/164426](https://doi.org/10.1086/164426)
- Lubow, S. H., & Ogilvie, G. I. 1998, *ApJ*, 504, 983, doi: [10.1086/306104](https://doi.org/10.1086/306104)
- Lubow, S. H., & Pringle, J. E. 1993, *ApJ*, 409, 360, doi: [10.1086/172669](https://doi.org/10.1086/172669)
- Lynden-Bell, D., & Kalnajs, A. J. 1972, *MNRAS*, 157, 1, doi: [10.1093/mnras/157.1.1](https://doi.org/10.1093/mnras/157.1.1)
- Lynden-Bell, D., & Pringle, J. E. 1974, *MNRAS*, 168, 603
- MacFadyen, A. I., & Milosavljević, M. 2008, *ApJ*, 672, 83, doi: [10.1086/523869](https://doi.org/10.1086/523869)
- Martin, R. G., Nixon, C. J., Pringle, J. E., & Livio, M. 2019, *NewA*, 70, 7, doi: [10.1016/j.newast.2019.01.001](https://doi.org/10.1016/j.newast.2019.01.001)
- McKee, C. F., & Ostriker, E. C. 2007, *ARA&A*, 45, 565, doi: [10.1146/annurev.astro.45.051806.110602](https://doi.org/10.1146/annurev.astro.45.051806.110602)
- Mendigutía, I., Calvet, N., Montesinos, B., et al. 2011, *A&A*, 535, A99, doi: [10.1051/0004-6361/201117444](https://doi.org/10.1051/0004-6361/201117444)
- Nidhi, S., Mathew, B., Shridharan, B., et al. 2023, *Monthly Notices of the Royal Astronomical Society*, 524, 5166, doi: [10.1093/mnras/stad2067](https://doi.org/10.1093/mnras/stad2067)
- Nixon, C., King, A., & Price, D. 2013, *MNRAS*, 434, 1946, doi: [10.1093/mnras/stt1136](https://doi.org/10.1093/mnras/stt1136)
- Nixon, C., & Lubow, S. H. 2015, *MNRAS*, 448, 3472, doi: [10.1093/mnras/stv166](https://doi.org/10.1093/mnras/stv166)
- Nixon, C. J. 2012, *MNRAS*, 423, 2597, doi: [10.1111/j.1365-2966.2012.21072.x](https://doi.org/10.1111/j.1365-2966.2012.21072.x)
- Nixon, C. J., Cossins, P. J., King, A. R., & Pringle, J. E. 2011a, *MNRAS*, 412, 1591, doi: [10.1111/j.1365-2966.2010.17952.x](https://doi.org/10.1111/j.1365-2966.2010.17952.x)
- Nixon, C. J., King, A. R., & Pringle, J. E. 2011b, *MNRAS*, 417, L66, doi: [10.1111/j.1745-3933.2011.01121.x](https://doi.org/10.1111/j.1745-3933.2011.01121.x)
- Orosz, J. A., Welsh, W. F., Carter, J. A., et al. 2012a, *ApJ*, 758, 87, doi: [10.1088/0004-637X/758/2/87](https://doi.org/10.1088/0004-637X/758/2/87)
- . 2012b, *Science*, 337, 1511, doi: [10.1126/science.1228380](https://doi.org/10.1126/science.1228380)
- Papaloizou, J., & Pringle, J. E. 1977, *MNRAS*, 181, 441, doi: [10.1093/mnras/181.3.441](https://doi.org/10.1093/mnras/181.3.441)
- Pelkonen, V.-M., Padoan, P., Juvela, M., Haugbølle, T., & Nordlund, Å. 2025, *A&A*, 694, A327, doi: [10.1051/0004-6361/202450682](https://doi.org/10.1051/0004-6361/202450682)

- Penzlin, A. B. T., Booth, R. A., Nelson, R. P., Schäfer, C. M., & Kley, W. 2024, *MNRAS*, 532, 3166, doi: [10.1093/mnras/stae1689](https://doi.org/10.1093/mnras/stae1689)
- Pierens, A., & Nelson, R. P. 2023, *A&A*, 670, A112, doi: [10.1051/0004-6361/202244828](https://doi.org/10.1051/0004-6361/202244828)
- Pinte, C., Ménard, F., Duchêne, G., et al. 2018a, *A&A*, 609, A47, doi: [10.1051/0004-6361/201731377](https://doi.org/10.1051/0004-6361/201731377)
- Pinte, C., Price, D. J., Ménard, F., et al. 2018b, *ApJL*, 860, L13, doi: [10.3847/2041-8213/aac6dc](https://doi.org/10.3847/2041-8213/aac6dc)
- Price, D. J., Wurster, J., Tricco, T. S., et al. 2018, *PASA*, 35, e031, doi: [10.1017/pasa.2018.25](https://doi.org/10.1017/pasa.2018.25)
- Pringle, J. E. 1981, *ARA&A*, 19, 137, doi: [10.1146/annurev.aa.19.090181.001033](https://doi.org/10.1146/annurev.aa.19.090181.001033)
- . 1991, *MNRAS*, 248, 754
- Pringle, J. E., & Rees, M. J. 1972, *A&A*, 21, 1
- Roedig, C., & Sesana, A. 2014, *MNRAS*, 439, 3476, doi: [10.1093/mnras/stu194](https://doi.org/10.1093/mnras/stu194)
- Rosotti, G. P. 2023, *NewAR*, 96, 101674, doi: [10.1016/j.newar.2023.101674](https://doi.org/10.1016/j.newar.2023.101674)
- Shakura, N. I., & Sunyaev, R. A. 1973, *A&A*, 24, 337
- Shi, J.-M., Krolik, J. H., Lubow, S. H., & Hawley, J. F. 2012, *ApJ*, 749, 118, doi: [10.1088/0004-637X/749/2/118](https://doi.org/10.1088/0004-637X/749/2/118)
- Smallwood, J. L., Franchini, A., Chen, C., et al. 2020, *MNRAS*, 494, 487, doi: [10.1093/mnras/staa654](https://doi.org/10.1093/mnras/staa654)
- Socia, Q. J., Welsh, W. F., Orosz, J. A., et al. 2020, *AJ*, 159, 94, doi: [10.3847/1538-3881/ab665b](https://doi.org/10.3847/1538-3881/ab665b)
- Stapper, L. M., Hogerheijde, M. R., van Dishoeck, E. F., et al. 2024, *A&A*, 682, A149, doi: [10.1051/0004-6361/202347271](https://doi.org/10.1051/0004-6361/202347271)
- Stassun, K. G., Mathieu, R. D., Mazeh, T., & Vrba, F. J. 1999, *AJ*, 117, 2941, doi: [10.1086/300881](https://doi.org/10.1086/300881)
- Sudarshan, P., Penzlin, A. B. T., Ziampras, A., Kley, W., & Nelson, R. P. 2022, *A&A*, 664, A157, doi: [10.1051/0004-6361/202243472](https://doi.org/10.1051/0004-6361/202243472)
- Tatulli, E., Isella, A., Natta, A., et al. 2007, *A&A*, 464, 55, doi: [10.1051/0004-6361:20065719](https://doi.org/10.1051/0004-6361:20065719)
- Teague, R., Bae, J., Aikawa, Y., et al. 2021, *ApJS*, 257, 18, doi: [10.3847/1538-4365/ac1438](https://doi.org/10.3847/1538-4365/ac1438)
- Thun, D., & Kley, W. 2018, *A&A*, 616, A47, doi: [10.1051/0004-6361/201832804](https://doi.org/10.1051/0004-6361/201832804)
- Welsh, W. F., Orosz, J. A., Carter, J. A., et al. 2012, *Nature*, 481, 475, doi: [10.1038/nature10768](https://doi.org/10.1038/nature10768)
- Welsh, W. F., Orosz, J. A., Short, D. R., et al. 2015, *ApJ*, 809, 26, doi: [10.1088/0004-637X/809/1/26](https://doi.org/10.1088/0004-637X/809/1/26)
- Wichittanakom, C., Oudmaijer, R. D., Fairlamb, J. R., et al. 2020, *MNRAS*, 493, 234, doi: [10.1093/mnras/staa169](https://doi.org/10.1093/mnras/staa169)
- Winn, J. N., Holman, M. J., Johnson, J. A., Stanek, K. Z., & Garnavich, P. M. 2004, *ApJL*, 603, L45, doi: [10.1086/383089](https://doi.org/10.1086/383089)
- Yamanaka, A., & Sasaki, T. 2019, *Earth, Planets, and Space*, 71, 82, doi: [10.1186/s40623-019-1064-0](https://doi.org/10.1186/s40623-019-1064-0)